Brillouin light scattering from quantized spin waves in nanowires with antisymmetric exchange interactions

Jun-Wen Xu,[1] Grant A. Riley,[2,4] Justin M. Shaw,[3] Hans T. Nembach,[2,5] and Andrew D. Kent[1,*]

[1]*Center for Quantum Phenomena, Department of Physics, New York University, New York, New York 10003, USA*
[2]*Associate, Physical Measurement Laboratory, National Institute of Standards and Technology, Boulder, Colorado 80305, USA*
[3]*Quantum Electromagnetics Division, National Institute of Standards and Technology, Boulder, Colorado 80305, USA*
[4]*Center for Memory and Recording Research, University of California - San Diego, La Jolla, California 92093, USA*
[5]*Department of Physics, University of Colorado, Boulder, Colorado 80309, USA*

(Received 14 July 2021; revised 20 December 2022; accepted 22 December 2022; published 7 February 2023)

Antisymmetric exchange interactions lead to nonreciprocal spin-wave propagation. As a result, spin waves confined in a nanostructure are not standing waves; they have a time-dependent phase, because counterpropagating waves of the same frequency have different wavelengths. We report on a Brillouin light scattering (BLS) study of confined spin waves in Co/Pt nanowires with strong Dzyaloshinskii-Moriya interactions. Spin-wave quantization in narrow ($\lesssim$200-nm-wide) wires dramatically reduces the frequency shift between BLS Stokes and anti-Stokes lines associated with the scattering of light incident transverse to the nanowires. In contrast, the BLS frequency shift associated with the scattering of spin waves propagating along the nanowire length is independent of nanowire width. A model that considers the chiral nature of modes captures this physics and predicts a dramatic reduction in frequency shift of light scattered from higher-energy spin waves in narrow wires, which is confirmed by our experiments.

DOI: 10.1103/PhysRevB.107.054402

I. INTRODUCTION

Antisymmetric exchange interactions fundamentally change the nature of spin-wave excitations and ground-state spin configurations. These interactions were first considered by Dzyaloshinskii [1] and Moriya [2] to explain the origin of the small magnetic moment in several uncompensated antiferromagnetic materials, which are now known as Dzyaloshinskii-Moriya interactions (DMIs). In contrast to Heisenberg exchange interactions, which lead to the collinear alignment of neighboring spins, DMI results in spin canting and chiral spin textures, such as magnetic skyrmions [3–5]. These topological magnetic objects are of intense interest in basic physics [6,7] and for possible racetrack memory devices [8–10].

A key characteristic of materials with DMI is nonreciprocal spin-wave propagation, with different wave vectors and characteristics for left and right propagating spin waves [11–18], i.e., the spin-wave dispersion is no longer symmetric about zero wave vector. The consequences of DMI are most directly observed in Brillouin light scattering (BLS) experiments in which photons create and annihilate spin waves with wave vectors collinear with the incident light. Since the wave vectors for these two processes have opposite signs, the frequency shift of the light is a direct measure of the nonreciprocal nature of the exchange interactions. For this reason, BLS is now a technique of choice for characterizing DMI [19].

The presence of DMI leads to interesting new physics in the case of confined spin waves [16]. Here, interference between counterpropagating spin waves cannot lead to standing waves, as left and right propagating waves at the same energy have different wavelengths. The quantized spin-wave modes also do not have space-inversion symmetry. The consequences of spin-wave quantization effects in the presence of DMI need to be studied experimentally.

In this paper, we present a Brillouin light scattering study of spin waves in nanowires with strong DMI. A dramatic reduction of the frequency shift between counterpropagating confined spin-wave modes occurs as the wire width is reduced. This is a direct consequence of the unusual non-standing-wave nature of the quantized spin-wave modes in the presence of chiral magnetic interactions.

The basics physics is illustrated in Fig. 1(a). In a nanostructure with chiral interactions, spin waves of the same frequency propagating in opposite directions have different wave-vector magnitudes, illustrated schematically by the orange and blue curves. The resulting interference pattern produced by these counterpropagating waves is thus neither symmetric nor antisymmetric about the midplane of the nanowire, as is the case for usual standing waves [16]. BLS can be used to determine the frequency shift associated with the inelastic scattering of light by spin waves, also known as magnons, i.e., a frequency shift caused by photon-magnon interactions. BLS is a powerful method to measure DMI in thin films and nanostructures [19–22]. This is because the frequency shift between counterpropagating spin waves is a direct consequence and measure of the strength of the chiral magnetic interactions. As shown in Fig. 1(a), *s*-polarized light is incident at an angle to the film normal and a magnetic field is applied in the film plane perpendicular to the light's plane of incidence, a configuration known as the Damon-Eshbach geometry. The light

*andy.kent@nyu.edu

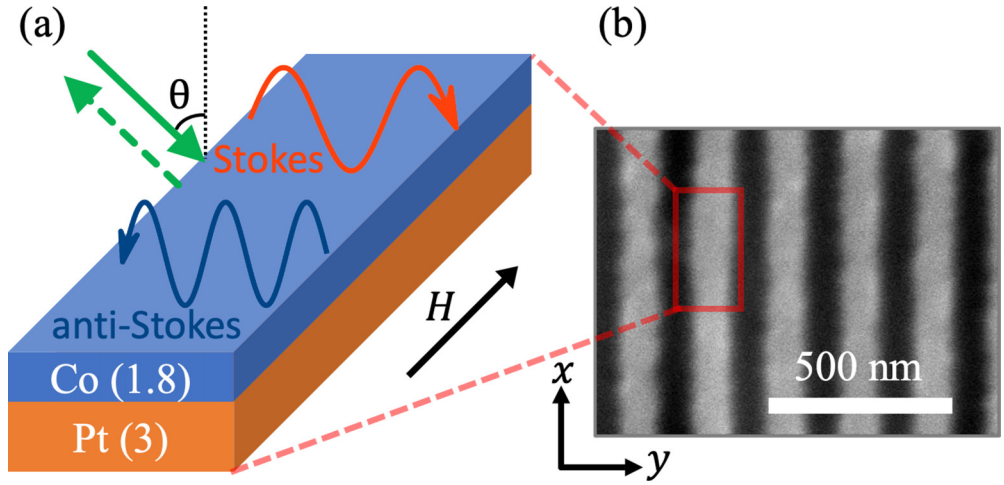

FIG. 1. (a) Schematic of spin waves in a confined geometry with chiral magnetic interactions. Left and right propagating spin waves of equal energy have different wave vectors, as indicated by the blue and orange colored waves. In BLS, *s*-polarized light with an angle of incidence θ, perpendicular to the applied field H, is backscattered by spin waves, as indicated by the green arrows. In a Stokes process, magnons with wave vectors moving away from the incident light are created, while in an anti-Stokes process, magnons of the opposite wave vectors are annihilated. (b) An SEM image of the nanowire array consisting of 100-nm-wide Co/Pt nanowires with 100 nm spacing. The nanowires are aligned in the x direction and their width is in the y direction.

backscattered from the sample is collected and analyzed. When the scattering process creates a magnon, the backscattered photon's frequency decreases (a Stokes process), whereas when a magnon is annihilated in the scattering process the frequency of the photon increases (an anti-Stokes process) [23]. By energy conservation, the shift of the photon frequency is the frequency of the excited or annihilated spin wave. The magnon momentum $\hbar q_{\mathrm{m}}$ is related to the angle of incidence of the light θ; momentum conservation gives $q_{\mathrm{m}} = (4\pi/\lambda)\sin\theta$, where λ is the wavelength of the light.

II. BRILLOUIN LIGHT SCATTERING EXPERIMENT

We conducted BLS on ferromagnetic nanowire arrays fabricated from Ta(4)/Pt(3)/Co(1.8)/Al(2)/Pt(3) thin films on oxidized silicon wafers, deposited using dc magnetron sputtering, with the numbers being the layer thicknesses in nanometers. The Pt/Co interface has been shown to induce a large DMI [24]. The Al layer decouples the Co layer and the Pt cap layer, which also protects the film from oxidation. Electron-beam lithography followed by Ar ion milling was used to define nanowire arrays and the width/spacing was varied from 100 to 400 nm. A scanning electron microscope (SEM) image of 100-nm-wide nanowires is shown in Fig. 1(b). Arrays are needed to have a sufficient filling factor for the BLS laser spot size[1].

Two different scattering geometries were used: A transverse geometry in which the incident light is perpendicular to the nanowire, as illustrated in Fig. 1(a), and a longitudinal geometry, where the incident light is parallel to the nanowire. BLS experiments were conducted with light of wavelength 532 nm at an incident angle of 45°, giving a momentum transfer $q_{\mathrm{m}} = 16.7\ \mu\mathrm{m}^{-1}$ (see Appendix A for results at different angles of incidence). Figures 2(a)–2(d) show the spectra of 400- and 100-nm nanowire arrays in these two geometries. The spectra indicate the Stokes (negative frequencies) and anti-Stokes (positive frequencies) lines for both field polarities. The scattering intensities are fit to find the peak positions and thus the frequency shift between the Stokes and anti-Stokes lines.

As noted, the frequency shift is a direct consequence of the spin-wave dispersion being asymmetric with respect to wave-vector inversion ($k \rightarrow -k$), i.e.,

$$f_k = f_0 + \frac{\gamma p D k}{\pi M_{\mathrm{s}}}, \tag{1}$$

where f_0 is the spin-wave frequency in the absence of the DMI, γ is the gyromagnetic ratio, M_{s} is the saturation magnetization, k is the spin-wave vector, $p = \pm 1$ indicates the magnetization polarity with respect to the x direction in the scattering geometry shown in Fig. 1, and D is the interfacial DMI. The frequency shifts as a function of wire width in the longitudinal and transverse geometries are shown in Fig. 2(e). In the longitudinal geometry, where the spin waves propagate along the nanowire, the frequency shift is independent of wire width. This is consistent with Eq. (1) and enables determination of the interfacial DMI from the frequency shift, with the known magnetization and gyromagnetic ratio [19]. The latter are determined using magnetometry and ferromagnetic resonance spectroscopy to be $M_{\mathrm{s}} = 9.39(1) \times 10^5$ A/m and $\gamma/2\pi = 30.3(1)$ GHz/T, respectively. We thus find the interfacial DMI to be $D = 4.79(7) \times 10^{-4}$ J/m^2. (Appendix A includes magnetic measurements and BLS results at different angles of incidence.)

[1]In principal micro-BLS could be used to study a single nanowire. However, its diffraction-limited resolution is of the order of 300 nm, which is not sufficient for our study. For spatially resolved images, a wire width of a few micrometers would be needed to have multiple data points across the standing wave. But spin-wave quantization effects for a micron width wire would be negligible.

However, in the transverse geometry, the frequency shift between the Stokes and anti-Stokes peak positions strongly depends on the nanowire width [Figs. 2(c) and 2(d)]; it decreases by more than a factor of 4 as the wire width varies from 400 to 100 nm [Fig. 2(e)]. This large reduction in the frequency shift cannot reflect changes in the DMI, as the DMI interaction is local; it is associated with exchange interactions and spin-orbit coupling on neighboring atoms at the Co/Pt interface [25]. Further, no changes in the spin-wave frequency shift were seen in the longitudinal scattering geometry, which would be affected if there were changes in the magnetic characteristics of the nanowires as their width is reduced.

III. ANALYSIS OF BRILLOUIN LIGHT SCATTERING RESULTS

Here, we show that the reduction in the BLS frequency shift in the transverse geometry is a direct consequence of the unusual nature of the quantized spin-wave modes in the presence of chiral magnetic interactions [16]. We consider only magnetic interactions within an individual nanowire, as interwire dipolar interactions are negligible compared to the intrawire exchange and DMI interactions [26]. To illustrate the essential physics, we consider the spin-wave dispersion relation [13,27,28]

$$f(k) = \frac{\gamma\mu_0}{2\pi}\left[\sqrt{\left(H + \frac{2A}{\mu_0 M_s}k^2 + P(|kt|)M_s\right)\left(H + \frac{2A}{\mu_0 M_s}k^2 - P(|kt|)M_s + M_{\text{eff}}\right)} + \frac{2pDk}{\mu_0 M_s}\right], \tag{2}$$

where μ_0 is the permeability of free space, t is the thickness of the magnetic layer, H is the applied field magnitude, A is the exchange constant, and M_{eff} is the effective magnetization, the demagnetization field minus the perpendicular anisotropy field associated with the Co/Pt interface K_p, $M_{\text{eff}} = M_s - 2K_p/(\mu_0 M_s)$. The coefficient $P(|kt|) = 1 - [1 - \exp(-|kt|)]/|kt|$ describes the dynamic demagnetizing interactions and reduces to $|kt|/2$ in the case of thin samples, i.e., for $kt \to 0$ [29]. We do not include the demagnetization factors in the nanowire width dimension as these do not come into the analysis of the BLS results (see Appendix D). $A = 2.27(1) \times 10^{-11}$ J/m and $M_{\text{eff}} = -7.35(8) \times 10^4$ A/m are determined from magnetization measurements and ferromagnetic resonance spectroscopy as discussed in Appendicies B and C.

In the y (the nanowire width) direction the spin-wave modes are confined and have quantized energies. At fixed frequency (or energy) the modes can be written as resulting from an interference pattern between left and right propagating spin waves, $\tilde{m}(y,t) = e^{-i2\pi f_k t} m(y)$, with $m(y)$, the y component of the magnetization, given by

$$m(y) = \frac{m_0}{2}\left[e^{ik_1(y+d/2)} + e^{ik_2(y+d/2)}\right], \tag{3}$$

where m_0 is the oscillation amplitude and $y \in [-d/2, d/2]$; the nanowire has a width d and spans from $-d/2$ to $d/2$ in the y direction. k_1 and k_2 are spin-wave vectors corresponding to spin waves propagating to the right and left (i.e., the sign of the wave vector is included in k_1 and k_2) with the same frequency f_k and thus energy. In the absence of DMI, the dispersion $f(k)$ is an even function of k, so $k_1 = -k_2$. With DMI the symmetry between counterpropagating spin-wave vectors is broken, causing $k_1 \neq -k_2$. Equation (3) can be written as

$$m(y) = \frac{m_0}{2}\left[e^{ik_1(y+d/2)} + e^{ik_2(y+d/2)}\right] \tag{4}$$

$$= m_0 \exp\left[\frac{i(k_1+k_2)}{2}(y+d/2)\right] \tag{5}$$

$$\times \cos\left[k_n(y+d/2)\right], \tag{6}$$

where

$$k_n = (k_1 - k_2)/2 = n\pi/d, \quad n = 0, 1, 2, \ldots \tag{7}$$

sets the quantization condition. Here, unpinned boundary conditions are assumed [28]. This form has an envelope (set by k_n) with a beat structure (given by $k_1 + k_2$) [16]. The gray horizontal lines in Figs. 3(a) and 3(b) indicate the quantized spin-wave frequencies for 400- and 100-nm-wide nanowires, respectively.

We now consider the scattering of light from these quantized modes. BLS is associated with magneto-optic effects in which light can be considered to be Bragg reflected from a phase grating created by spin waves. The differential light-scattering cross section for in-plane momentum transfer q is proportional to $I(q) = |m_q/m_0|^2$, where [28]

$$\frac{m_q}{m_0} = \frac{1}{m_0}\int_{-d/2}^{d/2} m(y)e^{-iqy}dy = \frac{d}{2}\left\{e^{ik_1 d/2}\,\text{sinc}\left[\frac{1}{2}(k_1 - q)d\right] + e^{ik_2 d/2}\,\text{sinc}\left[\frac{1}{2}(k_2 - q)d\right]\right\}, \tag{8}$$

and $\text{sinc}\, x \equiv \sin x/x$. For quantized spin waves described by Eq. (6) the normalized BLS intensity is given by

$$I_n(q,d) = \frac{d^2}{4}\left\{\text{sinc}\left[\frac{1}{2}(k_1 - q)d\right] + (-1)^n \text{sinc}\left[\frac{1}{2}(k_2 - q)d\right]\right\}^2, \tag{9}$$

where k_1 and k_2 are set by the quantization condition [Eq. (7)]. Equation (9) includes terms of the form of sinc functions. This means that if k were a continuous variable (not quantized), the intensity would be maximum when $k_1 = q_m$ for the Stokes process and $k_2 = -q_m$ for the anti-Stokes process, indicated by the blue and orange squares in Figs. 3(a) and 3(b).

Figures 3(c)–3(f) show the normalized intensities calculated for each quantized mode n using Eq. (9) for 400- and 100-nm nanowires both for Stokes and anti-Stokes processes. The results are shown as bar graphs. For the 400-nm sample, the maximum intensities occur for the $n = 0$ mode for the Stokes process and $n = 3$ for the anti-Stokes process. Their frequency difference is very close to that expected in the continuum limit, indicated by the dashed blue and orange vertical lines. However, for the 100-nm nanowire, the maximum scattering intensities for both the Stokes and the anti-Stokes processes are associated with the $n = 0$ mode. As a result, the frequency difference between the maxima is zero, i.e., in

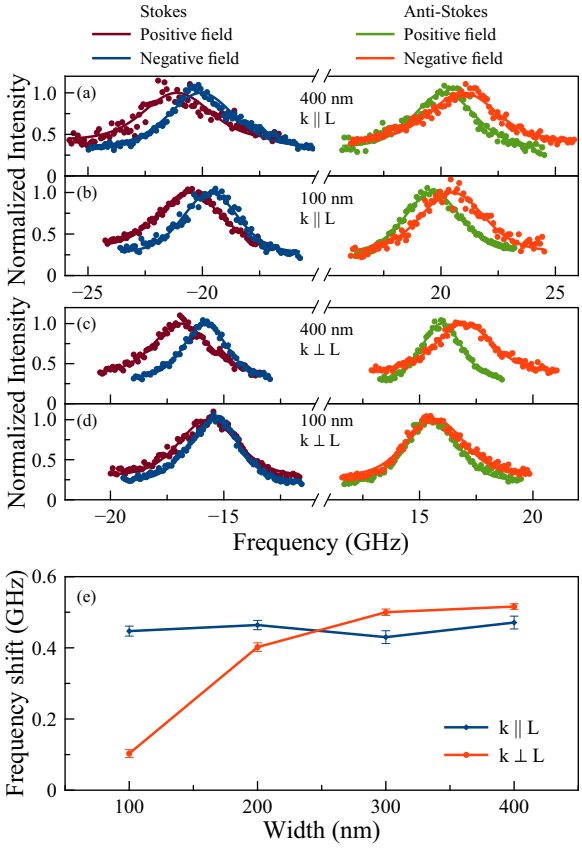

FIG. 2. (a)–(d) BLS spectra for Stokes and anti-Stokes processes for both positive and negative fields on nanowire arrays with different widths. (e) The absolute value of the frequency shift on nanowire arrays with different widths in the longitudinal ($k \parallel L$) and transverse ($k \perp L$) scattering geometries. In the longitudinal geometry the frequency shift is independent of nanowire width, whereas in the transverse geometry the frequency shift decreases significantly in narrow wires. The magnetic fields applied $\mu_0 H$ for longitudinal and transverse scattering geometries are 0.784 and 0.578 T, respectively.

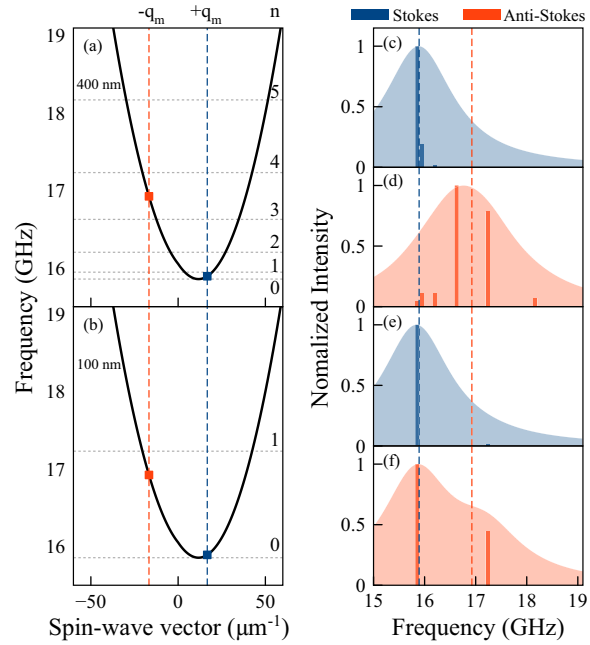

FIG. 3. Spin-wave dispersion for (a) 400-nm and (b) 100-nm nanowires based on Eq. (2) for negative field polarity ($p = -1$). The vertical lines indicate the transferred wave vector q_m for both Stokes and anti-Stokes processes. The blue and orange squares at the intersection of $\pm q_m$ with the dispersion curve are the BLS peak positions for Stokes and anti-Stokes process in the continuum ($d \to \infty$) limit. The gray horizontal lines indicate the frequencies of quantized spin waves, with their indices n labeled on the right-hand side. (c)–(f) Bar graphs of the BLS light scattering intensities for the quantized modes I_n in Eq. (9) for (c), (d) 400-nm and (e), (f) 100-nm nanowires, respectively. The blue figures are Stokes processes, and the orange figures are anti-Stokes processes. The blue and orange vertical dashed lines indicate the frequencies in a continuous ($d \to \infty$) limit, shown as squares in (a) and (b). Spin-wave quantization in the narrowest nanowire leads to the scattering intensity being largest for the lowest-frequency $n = 0$ mode, the most uniform mode, which leads to a reduced BLS frequency shift. The shaded colors show the spectra including the finite spin lifetime.

both cases maximum scattering intensity is associated with the lowest frequency and the most spatially uniform mode.

This is the basic physics: Spin-wave quantization leads to the BLS light scattering from the narrowest nanowire being dominated by the lowest frequency and the most uniform mode, which is least affected by DMI, because of its small wave vector. To make a more quantitative comparison between the model and experiment, we consider the lifetime of the modes by convoluting the intensities associated with the quantized modes with a Lorentzian determined by the mode lifetime, set by the damping (see Appendix E). The shaded colors in Figs. 3(c)–3(f) are the resulting intensity profiles. After considering the spin state lifetimes, we determine and plot the resulting peak frequency shift versus wire width. This is shown in Fig. 4(b) next to the experimental results in Fig. 4(a). The model captures the experimental trends well.

IV. DISCUSSION: EXPERIMENT AND MODEL

It is clear that damping broadens the spectra so that it is not possible to observe distinct peaks associated with the quantized modes. This is a consequence of the experimental requirement of having a large DMI; a large DMI requires the ferromagnetic layer to be thin and spin pumping in such layers increases the damping significantly [30]. This would be the case independent of the intrinsic damping of the ferromagnetic layers (which can be very low in transition metal alloys [31]). Increased damping is also founded in other studies of nanostructured samples [32]. Furthermore, the broad peaks may also partly be a result of inhomogeneous broadening, as we are measuring an array of nanowires, instead of a single nanowire. The model further predicts that the decrease of the BLS frequency shift is mainly associated with a reduction in the frequency of the anti-Stokes peak. The experimental results are shown in Fig. 4(c) and the model results are in Fig. 4(d). The anti-Stokes frequency is indeed a much stronger function of the nanowire width than the Stokes peak. We note that the frequency of the Stokes peak decreases with decreasing wire width more than seen in the model. This can be a consequence of the approximate spin-wave dispersion

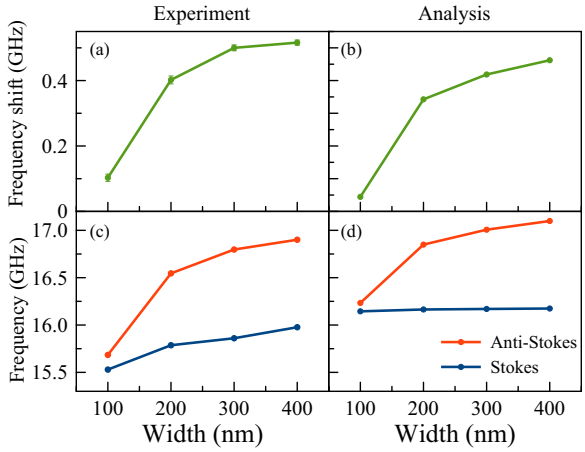

FIG. 4. (a) Measured BLS frequency shift for different nanowire widths. (b) Frequency shift determined from the quantized spin-wave model. (c) The measured BLS Stokes and anti-Stokes peak frequencies for negative field polarity. (d) Model peak frequencies for both Stokes and anti-Stokes processes; the model predicts a stronger decrease in the anti-Stokes frequency which is observed in the experiment.

relation used; the magnon wave vector $-q_{\mathrm{m}}$ may not be as close to the bottom of the spin-wave band as in the model. As a result, spin-wave quantization will lead to a reduction in the frequency of the mode with decreasing wire width. On reversing the field ($p = -1 \rightarrow p = +1$) the situation is reversed: The Stokes peak is now the higher-frequency mode and its BLS spectra are more strongly affected by wire width. These characteristics taken together are strong evidence that our model is capturing the essential physics.

V. SUMMARY

In summary, DMI in combination with the unusual nature of confined spin-wave modes in nanowires leads to a strong decrease in the frequency shift in light scattered by counterpropagating modes. The strong frequency reduction is associated with mode quantization of quantized spin waves in the presence of DMI. This demonstrates that, in contrast to the BLS frequency shift in the longitudinal scattering geometry, which enables direct determination of the DMI [19], the BLS frequency shift in the transverse scattering geometry is not directly related to the DMI. This observation also raises the question of how such spin-wave quantization affects other nanowire magnetic properties, such as skyrmions and domain wall dynamics in racetracks. More generally, this physics is important for understanding spin waves in confined systems and characterizing antisymmetric exchange interactions in magnetic racetracks and other types of magnetic nanostructures that lack inversion symmetry.

ACKNOWLEDGMENTS

This work was supported in part by the DARPA Topological Excitations in Electronics (TEE) program (Grant No. D18AP00009). A.D.K. also acknowledges support from NSF DMR-2105114. The nanostructures were realized at the Advanced Science Research Center NanoFabrication Facility of the Graduate Center at the City University of New York.

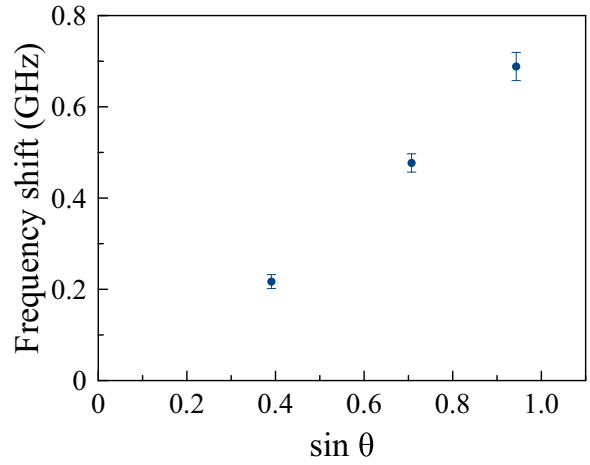

FIG. 5. BLS frequency shift vs sine of the incident angle for the 400-nm nanowire array in the transverse scattering geometry.

APPENDIX A: BLS RESULTS FOR DIFFERENT ANGLES OF INCIDENCE

We conducted BLS measurements in the transverse geometry for several different angles of incidence $\theta = 23^\circ, 45^\circ, 71^\circ$, to vary the in-plane wave vector q_{m}. According to Eq. (1) in the main text, the frequency shift is proportional to the transferred wave vector q_{m}, and thus to $\sin\theta$. In Fig. 5, we plot the frequency shift for the 400-nm nanowire array versus $\sin\theta$, which shows the expected linear relation.

In Fig. 6, we plot the BLS frequency shift for nanowire arrays with different widths and different angles of incidence, again in the transverse scattering geometry. As with the $\theta = 45^\circ$ results discussed in the main text, a dramatic decrease in the frequency shift occurs when the nanowire width is less than 200 nm.

Lastly, in Fig. 7 we plot the Stokes and anti-Stokes peak frequencies for different nanowire widths and angles of

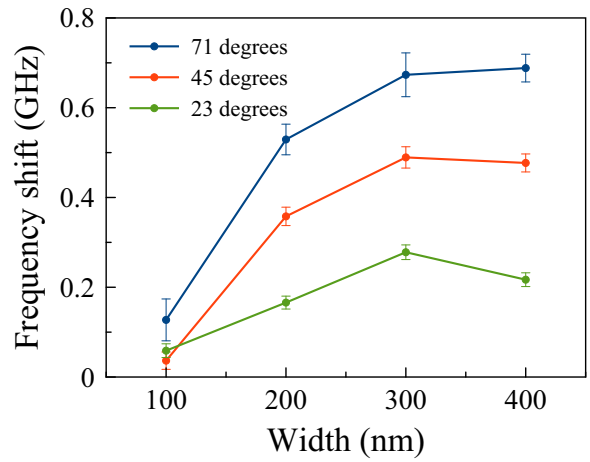

FIG. 6. Nanowire width vs frequency shift for different incident angles in the transverse scattering geometry.

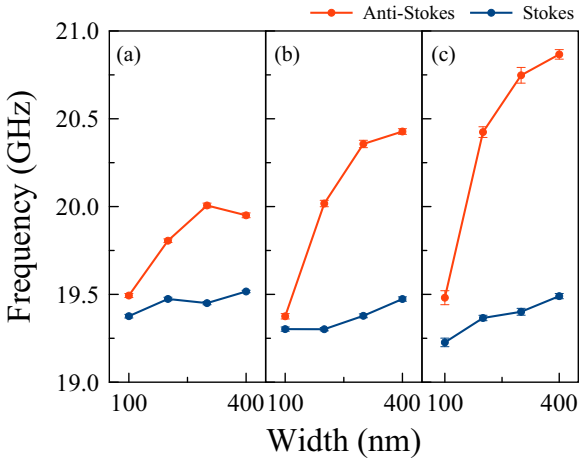

FIG. 7. The Stokes and anti-Stokes peak frequencies for different nanowire widths for (a) $\theta = 23°$, (b) $\theta = 45°$, and (c) $\theta = 71°$ at a negative applied field, $p = -1$.

incidence. As we showed in Fig. 4 in the main text, the major contribution to the decrease in the frequency shift comes from decreasing frequency of the anti-Stokes peak for this polarity of the applied field ($p = -1$).

APPENDIX B: FERROMAGNETIC RESONANCE SPECTROSCOPY

Ferromagnetic resonance (FMR) spectroscopy was conducted with a vector network analyzer (VNA). The unpatterned film was diced and placed on a coplanar waveguide (CPW). Polymethyl methacrylate (PMMA) was spun on the film's surface to prevent direct electrical contact to the CPW. We applied a microwave signal to the CPW at a fixed frequency and swept the external magnetic field perpendicular to the film plane. We then fit the complex transmission parameter S_{21} to determine the resonance frequency and linewidth [33]. The out-of-plane resonance field and frequency follow the Kittel relation,

$$f = \frac{\mu_0 \gamma}{2\pi}(H - M_{\text{eff}}), \tag{B1}$$

where γ is the gyromagnetic ratio, μ_0 is the permeability of free space, and M_{eff} is the effective magnetization. The linewidth versus frequency gives information on the damping,

$$\mu_0 \Delta H = \frac{4\pi\alpha f}{\gamma} + \mu_0 \Delta H_0, \tag{B2}$$

where α is Gilbert damping constant and $\mu_0 \Delta H_0$ is the inhomogeneous linewidth broadening. Figure 8 shows the results with the fits to Eqs. (B1) and (B2). We find $\gamma/2\pi = 30.3(1)$ GHz/T, $M_{\text{eff}} = -7.35(8) \times 10^4$ A/m, and $\alpha = 0.0230(8)$.

APPENDIX C: SQUID MAGNETOMETRY

We used a superconducting quantum interference device (SQUID) magnetometer to measure the film's saturation magnetization. At room temperature, $M_s = 9.39(1) \times 10^5$ A/m. In order to determine the exchange constant A, we measured

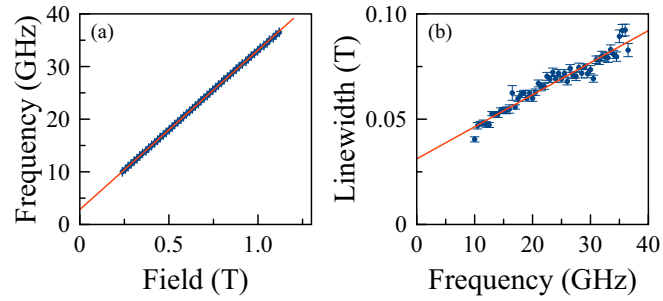

FIG. 8. (a) FMR frequency vs resonance field in the field perpendicular geometry. The blue points are the experimental data and the orange line is a fit of the data to Eq. (B1). (b) FMR linewidth vs frequency. The blue points are the data and the orange line is a fit to Eq. (B2).

the temperature dependence of the saturation magnetization $M_s(T)$, as shown in Fig. 9. According to the Bloch $T^{3/2}$ law [34], the temperature dependence follows the relation

$$M_s(T) = M_s(0)\left[1 - \frac{g\mu_B \eta}{M_s(0)}\left(\frac{k_B T}{D_{\text{spin}}(0)}\right)^{\frac{3}{2}}\right], \tag{C1}$$

where $D_{\text{spin}}(T)$ is the spin-wave stiffness, g is the Landé g factor, μ_B is the Bohr magneton, and $\eta = 0.0587$ is a dimensionless constant that depends on the sample geometry. In mean-field theory [35], the temperature-dependent spin-wave stiffness is given by

$$D_{\text{spin}}(T) = \frac{M_s(T)}{M_s(0)} D_{\text{spin}}(0). \tag{C2}$$

Then, we can calculate the exchange stiffness according to the equation

$$A(T) = \frac{M_s(T) D_{\text{spin}}(T)}{2g\mu_B}, \tag{C3}$$

and find $A = 2.27(1) \times 10^{-11}$ J/m at 300 K. Further details on this analysis can be found in Ref. [19].

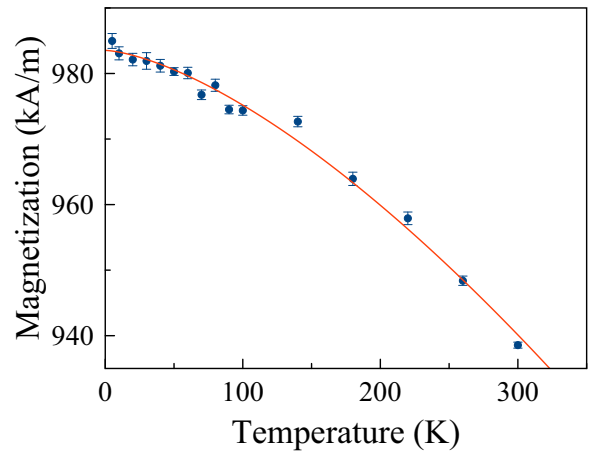

FIG. 9. Saturation magnetization vs temperature. The blue points are the data and the orange line is a fit to Eq. (C1), which is used to determine the exchange constant A.

APPENDIX D: WIDTH DEPENDENCE OF DEMAGNETIZATION FACTORS

We did not include the width dependence of the nanowire's demagnetization factors into the analysis for several reasons. First, the demagnetization factors change the frequency for the Stokes and anti-Stokes processes in the same manner and thus do not affect the frequency shift caused by DMI. Second, only the frequency of the lowest mode ($n = 0$) is effected, and the effect is negligible for all modes with higher indices (i.e., $n \geqslant 1$) [28]. Lastly, in our study, the Co thickness is only 1.8 nm, which is much smaller than the width of the nanowires. The width direction demagnetization factors calculated using a cuboid model are only 3.2% for the 100-nm nanowires and 1.0% for the 400-nm nanowires. Therefore, ignoring the width direction demagnetization fields does not affect our analysis.

APPENDIX E: LIFETIME BROADENING OF BLS SPECTRA

The lifetime of the spin-wave modes is limited by the magnetic damping. To consider the spin-wave lifetime in our analysis and model, we broaden the model intensities I_n in Eq. (7) of the main text by including the lifetime of the spin-wave modes. First, the discretized intensity can be written as

$$I(f) = \sum_{n=0}^{\infty} I_n \delta(f - f_n), \tag{E1}$$

where $\delta(f - f_n)$ is the Dirac delta function. We then convolute the delta function with a Lorentzian function of the form

$$L_n(f) = \frac{1}{(f - f_n)^2 + \left(\frac{\Delta f_n}{2}\right)^2}. \tag{E2}$$

The mode lifetime is set by the Gilbert damping constant, Eq. (B2), and thus $\Delta f_n = \Delta H \frac{df}{dH}|_{f=f_n}$, i.e., we convert the linewidth in field to a frequency linewidth. The curves shown in Figs. 3(c)–3(f) in the main text, before normalization, are then given by

$$I(f) = \sum_{n=0}^{\infty} \frac{I_n}{(f - f_n)^2 + \left(\frac{1}{2}\Delta H \frac{df}{dH}\big|_{f=f_n}\right)^2}, \tag{E3}$$

where $\mu_0 \Delta H$ is the linewidth taken from the FMR experiment.

[1] I. Dzyaloshinsky, J. Phys. Chem. Solids **4**, 241 (1958).
[2] T. Moriya, Phys. Rev. **120**, 91 (1960).
[3] A. Fert, N. Reyren, and V. Cros, Nat. Rev. Mater. **2**, 17031 (2017).
[4] F. Büttner, I. Lemesh, M. Schneider, B. Pfau, C. M. Günther, P. Hessing, J. Geilhufe, L. Caretta, D. Engel, B. Krüger *et al.*, Nat. Nanotechnol. **12**, 1040 (2017).
[5] L. Caretta, M. Mann, F. Büttner, K. Ueda, B. Pfau, C. M. Günther, P. Hessing, A. Churikova, C. Klose, M. Schneider *et al.*, Nat. Nanotechnol. **13**, 1154 (2018).
[6] U. K. Roessler, A. N. Bogdanov, and C. Pfleiderer, Nature (London) **442**, 797 (2006).
[7] M. Uchida, Y. Onose, Y. Matsui, and Y. Tokura, Science **311**, 359 (2006).
[8] S. S. P. Parkin, M. Hayashi, and L. Thomas, Science **320**, 190 (2008).
[9] R. Tomasello, E. Martinez, R. Zivieri, L. Torres, M. Carpentieri, and G. Finocchio, Sci. Rep. **4**, 1 (2014).
[10] S. Parkin and S.-H. Yang, Nat. Nanotechnol. **10**, 195 (2015).
[11] A. N. Bogdanov and U. K. Rößler, Phys. Rev. Lett. **87**, 037203 (2001).
[12] D. Cortés-Ortuño and P. Landeros, J. Phys.: Condens. Matter **25**, 156001 (2013).
[13] J.-H. Moon, S.-M. Seo, K.-J. Lee, K.-W. Kim, J. Ryu, H.-W. Lee, R. D. McMichael, and M. D. Stiles, Phys. Rev. B **88**, 184404 (2013).
[14] K. Di, V. L. Zhang, H. S. Lim, S. C. Ng, M. H. Kuok, X. Qiu, and H. Yang, Appl. Phys. Lett. **106**, 052403 (2015).
[15] J. M. Lee, C. Jang, B.-C. Min, S.-W. Lee, K.-J. Lee, and J. Chang, Nano Lett. **16**, 62 (2016).
[16] B. W. Zingsem, M. Farle, R. L. Stamps, and R. E. Camley, Phys. Rev. B **99**, 214429 (2019).
[17] H. Wang, J. Chen, T. Liu, J. Zhang, K. Baumgaertl, C. Guo, Y. Li, C. Liu, P. Che, S. Tu *et al.*, Phys. Rev. Lett. **124**, 027203 (2020).
[18] J. Lucassen, C. F. Schippers, M. A. Verheijen, P. Fritsch, E. J. Geluk, B. Barcones, R. A. Duine, S. Wurmehl, H. J. M. Swagten, B. Koopmans, and R. Lavrijsen, Phys. Rev. B **101**, 064432 (2020).
[19] H. T. Nembach, J. M. Shaw, M. Weiler, E. Jué, and T. J. Silva, Nat. Phys. **11**, 825 (2015).
[20] K. Di, V. L. Zhang, H. S. Lim, S. C. Ng, M. H. Kuok, J. Yu, J. Yoon, X. Qiu, and H. Yang, Phys. Rev. Lett. **114**, 047201 (2015).
[21] A. A. Stashkevich, M. Belmeguenai, Y. Roussigné, S. M. Cherif, M. Kostylev, M. Gabor, D. Lacour, C. Tiusan, and M. Hehn, Phys. Rev. B **91**, 214409 (2015).
[22] Y. Quessab, J.-W. Xu, C. T. Ma, W. Zhou, G. A. Riley, J. M. Shaw, H. T. Nembach, S. J. Poon, and A. D. Kent, Sci. Rep. **10**, 7447 (2020).
[23] G. Gubbiotti, S. Tacchi, M. Madami, G. Carlotti, A. O. Adeyeye, and M. Kostylev, J. Phys. D **43**, 264003 (2010).
[24] M. Belmeguenai, J.-P. Adam, Y. Roussigné, S. Eimer, T. Devolder, J.-V. Kim, S. M. Cherif, A. Stashkevich, and A. Thiaville, Phys. Rev. B **91**, 180405(R) (2015).
[25] S. Kim, K. Ueda, G. Go, P.-H. Jang, K.-J. Lee, A. Belabbes, A. Manchon, M. Suzuki, Y. Kotani, T. Nakamura *et al.*, Nat. Commun. **9**, 1 (2018).

[26] G. Gubbiotti, S. Tacchi, G. Carlotti, P. Vavassori, N. Singh, S. Goolaup, A. O. Adeyeye, A. Stashkevich, and M. Kostylev, Phys. Rev. B **72**, 224413 (2005).

[27] B. A. Kalinikos and A. N. Slavin, J. Phys. C **19**, 7013 (1986).

[28] J. Jorzick, S. O. Demokritov, C. Mathieu, B. Hillebrands, B. Bartenlian, C. Chappert, F. Rousseaux, and A. N. Slavin, Phys. Rev. B **60**, 15194 (1999).

[29] H. Bouloussa, J. Yu, Y. Roussigné, M. Belmeguenai, A. Stashkevitch, H. Yang, and S. Chérif, J. Phys. D **51**, 225005 (2018).

[30] C. T. Boone, J. M. Shaw, H. T. Nembach, and T. J. Silva, J. Appl. Phys. **117**, 223910 (2015).

[31] M. A. W. Schoen, D. Thonig, M. L. Schneider, T. J. Silva, H. T. Nembach, O. Eriksson, O. Karis, and J. M. Shaw, Nat. Phys. **12**, 839 (2016).

[32] J. M. Shaw, T. J. Silva, M. L. Schneider, and R. D. McMichael, Phys. Rev. B **79**, 184404 (2009).

[33] H. T. Nembach, T. J. Silva, J. M. Shaw, M. L. Schneider, M. J. Carey, S. Maat, and J. R. Childress, Phys. Rev. B **84**, 054424 (2011).

[34] C. A. F. Vaz, J. A. C. Bland, and G. Lauhoff, Rep. Prog. Phys. **71**, 056501 (2008).

[35] U. Atxitia, O. Chubykalo-Fesenko, N. Kazantseva, D. Hinzke, U. Nowak, and R. W. Chantrell, Appl. Phys. Lett. **91**, 232507 (2007).